A Multi-resolution Experimental Methodology for Fatigue Mechanism Verification of Physics-based Prognostics

Jian Yang, Wei Zhang, and Yongming Liu

Department of Civil and Environmental Engineering, Clarkson University, Potsdam, NY, 13699, USA

jiyang@clarkson.edu
zhangw@clarkson.edu
yliu@clarkson.edu

ABSTRACT

An experimental methodology is proposed in this paper for mechanism verification of physics-based prognosis of mechanical damage, such as fatigue. The proposed experimental methodology includes multi-resolution in-situ mechanical testing, advanced imaging analysis, and mechanism analysis based on digital measurements. A case study is presented for fatigue crack growth mechanism investigation. In-situ fatigue testing at lower resolutions, i.e., optical microscopy, and digital image correlation is used to analyze the plastic deformation behavior and strain distribution near crack tips. In-situ fatigue testing under higher resolutions, i.e., scanning electron microscopy, and automatic image tracking is used to obtain detailed crack tip deformation and crack growth kinetics at the nanometer scales. Following this, the proposed experimental methodology is applied to two different metallic materials, aluminum alloys and steels. Very different experimental observations are observed and the underlying mechanisms are discussed in detail. The impact on the prognosis algorithm development is also discussed. Finally, the potential application of the proposed experimental methodology to other materials systems and to other types of mechanical damage is discussed.

1. INTRODUCTION

Structural damage prognosis mainly relies on two kinds of methods: data-driven methods and physical-based methods. Though they are often combined in application, the physical based method is much more precise and flexible for new loading condition even new systems with a similar mechanism (Farrar & Lieven, 2007). Among the various structural failures modes, fatigue caused failure is a main failure mode of structures under cyclic loading and it can have catastrophic consequences, with loss of life and property (Campbell & Lahey, 1984).

The theory of metal fatigue has been developed for a long time. In 1962, Forsyth first gives a detail of the two stages in fatigue initialization and propagation (Forsyth, 1962). In stage I, when the initial crack length is less than a few grain diameters, an initial stress is required to open the crack as it might be fully closed, and additional stress is applied for crack propagation. In stage II, the crack growth process involves simultaneous or alternating flow along two slip system and it largely depend on the stress intensity at the crack tip. Paris' law (Paris, Gomez, & Anderson, 1961) gives a power relationship between fatigue crack growth rate and stress intensity range of constant amplitude loading. However, when considering the failure physics, the crack does not propagate throughout the whole unloading cycle, though the unloading has a sharpening effect to the rack tip (Laird, 1967). Moreover, when the stress is removed, the residual plastic region may force the crack close fully at the crack tip (Wolf, 1970). However, many experiments show the difficulties in measuring the crack-opening load, depending on the measuring location (Macha, Corbly, & Jones, 1979) and the techniques employed, such as by electrical potential method (Shih and Wei 1974), by ultrasonic method (Bouami & De Vadder, 1986; Singh, Srivastav, Gupta, Keller, & Ray, 2009), and numerical method (Riddell, Piascik, Sutton, Zhao, McNeill & Helm, 1999). Further, it is found that commonly employed notch-mouth clip-gauge method is not sensitive enough to detect the closure of short cracks in regions of notch plasticity (Fleck & Shin, 1985) and changes in the stresses ahead of the crack tip are more important than closure behind the crack tip (Sadananda, 1999).

For crack closure hypothesis, many experimental studies are based on the indirect measurement and there lacks a method for the direct model verification at various different scales. The mechanism/hypothesis verification is critical for a

sound physics-based prognosis framework and must be carefully investigated.

In this paper, a multi-resolution in-situ testing methodology is proposed for the mechanism/hypotheses verification for mechanical damage prognosis. The proposed methodology combines advanced experimental instrumentation, digital imaging technique, and mechanical analysis to investigate the mechanical deformation and damage progression behavior under mechanical loadings at two scales, micrometer scale (optical) and nanometer scale (SEM). The two experimental testing results are compared and verified each other for non-closure hypotheses. The application in two materials show significantly different fatigue behaviors and the direct observations at nanometer to millimeter scales provide fruitful information for the new model development and model hypothesis verification.

This paper is organized as follows. First, the in-situ experiment methodology and the detail steps are introduced. In-situ fatigue testing at lower resolutions, i.e., optical microscopy, and digital image correlation is used to analyze the plastic deformation behavior and strain distribution near crack tips. In-situ fatigue testing under higher resolutions, i.e., scanning electron microscopy, and automatic image tracking is used to obtain detailed crack tip deformation and crack growth kinetics at the nanometer scales. Following this, the proposed experimental methodology is applied to two different metallic materials, e.g., aluminum alloys and steels. Very different experimental observations are observed and the underlying mechanisms are discussed in detail. The impact on the prognosis algorithm development is also discussed. Finally, the potential application of the proposed experimental methodology to other materials systems and to other types of mechanical damage is discussed.

2. IN-SITU OPTICAL EXPERIMENT

2.1. Experiment Setup

The experimental set-up for the in-situ optical microscopy experiment is shown in Fig. 1. The experimental instrument mainly includes two parts: a palm-sized loading system and an optical microscope system. The tensile stage is manufactured by Fullerm Inc. (now MTI) and the maximum gage length between mechanical grips is about 27 mm. The load capacity is 5 kN. The sub-stage is fixed on the microscope and the cyclic loading is applied to the specimen. The testing is controlled by the Admet MTESTQuattro system. A Nikon metallurgical microscope is used to monitor the specimen surface and a high resolution imaging acquisition system is used to record images during the testing. Post-processing of images is performed using a high performance workstation and the software package ImageJ

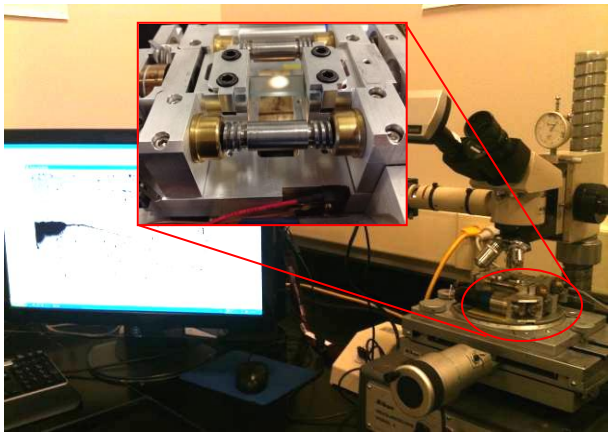

Fig. 1 Experiment setup

Single edge notched plate specimens with width W = 8.1 mm, length L = 52 mm and thickness 0.86 mm made of aluminum alloy sheet (7075-T6) were tested. An edge notch of length 1mm was machined on specimen by slow saw cutting. After machining, the specimens are pre-cracked under a hydraulic tension machine INSTRON 1331 until the initial crack reaches about 1 mm. The pre-cracking procedure follows the ASTM standard E647-99. Following this, both surfaces of the specimen are polished with the sandpaper whose average particle diameter is smaller than 10 um. The final polishing is done using a vibration polishing machine with 1~3um polishing suspension.

2.2. Test Procedure

The experiment consists of four major steps:

1. Specimen manufacturing and pre-cracking.
2. Polish the specimen carefully to form randomly distributed small dark regions on the smooth surface, which is a requirement for digital image correlation (DIC) analysis.
3. Apply load on the specimen under the monitoring of a microscope, while images of the crack tip region are taken during the loading and unloading process.
4. process the images by DIC software to get the strain field of the crack tip region and calculate the plastic zone using mechanical analysis.

In the experiment, a load cycle is divided into several steps in the load profile. At each step, the image around the crack region is taken for strain calculation. The step load is set according to the precision requirement and computation resource limitation. An example profile is shown in Fig. 2, which has about forty segments during the loading and unloading path.

2.3. Test Procedure

Before the images are processed using VIC-2D for strain calculation, some pre-processes are required depending on

the image quality. The most common process is the contrast enhancement. The raw images may not be sharp enough for DIC calculation and enhancing the contrast could make the pixels easy to be recognized. In addition, it could also mitigate the negative effect of blur edge by out of focus.

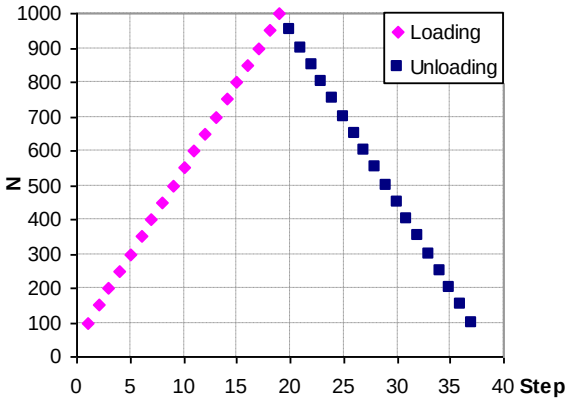

Fig. 2 Load profile

After the image pre-processing, digital image correlation can be used to estimate the strain and displacement of the region of interest. The obtained strain field is used for the mechanical and damage analysis.

In fatigue, plastic deformation is one of the most important factors affecting damage accumulation. Thus, the focus in this paper is on the plastic zone estimation. Under cyclic loading, the crack closure during the reverse loading path (or the crack opening level during the loading path) will be critical for fatigue analysis. Some previous studies have shown the crack closure level and crack opening level are very close and can be assumed to be equal (Zhang & Liu, 2011). The identification during the reverse loading path will be sufficient to estimate this value. It should be noted that the proposed experimental methodology is not limited to fatigue and other types of mechanical damage can be analyzed using the obtained strain field as well.

The theoretical reversed plastic zone under cyclic loading can be estimated by Eq. (1) without the consideration of crack closure (Rice, 1968)

$$\rho = \frac{1}{\pi}\left(\frac{\Delta K}{2\sigma_y}\right)^2 \tag{1}$$

where σ_y is the yielding strength and

$$\Delta K = F \cdot \Delta\sigma\sqrt{\pi a} = F \cdot \left(\sigma_{\max} - \sigma_{\min}\right)\sqrt{\pi a} \tag{2}$$

where F is the geometry factor which depends on the geometry of specimen and the crack length. a is the crack length. A sample contour of strain field in front of the crack is shown in Fig. 3(a), the crack grows from the center of left edge. The calculated plastic zone is shown as the red region in Fig. 3 (b). Finally, the plastic zone size is defined along the crack propagation direction and it can be measured directly from the processed image.

By repeating the above procedures for images taken at different loading levels, the strain field and plastic zone evolution can be obtained. By comparing the experimental observations with theoretical model predictions (for example, Eq. (1), the hypothesis of the model can be justified.

In-situ optical testing has the resolution limit to about 0.5~5 microns. If more detailed information of the materials at finer resolution is desired, new imaging capabilities is required. In-situ SEM testing is required and is discussed below.

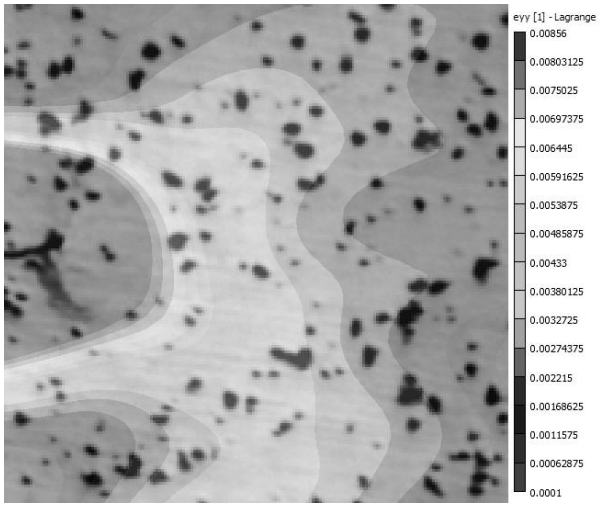

(a) Strain couture from VIC-2D

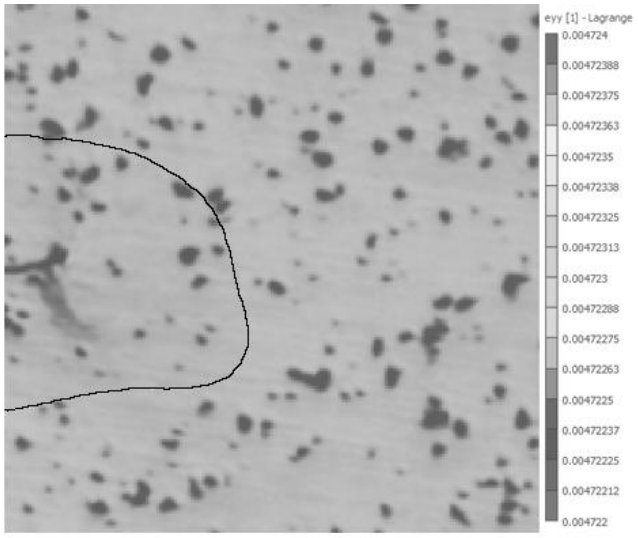

(b) Plastic zone from VIC-2D

Fig. 3 Strain field and plastic zone from VIC-2D

3. IN-SITU SEM EXPERIMENT

3.1. Experiment Setup

The process of in-situ SEM experiment is the similar with optical experiment. The palm-sized loading machine is put in a scanning electron microscope for imaging (JEOL-7400F SEM in the current investigation). The experimental setup is in shown in Fig. 4.

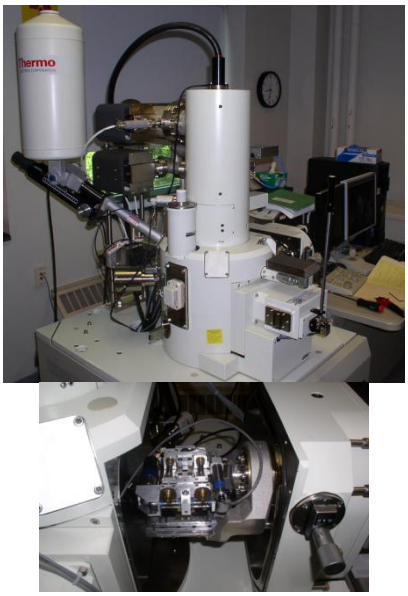

Fig. 4 SEM experiment set up

3.2. Test Procedure

The load profile is the same with optical experiment. There is a minor difference. Under the optical observation, the lens field depth is large enough to cover the specimen moving distance. Thus, the images can be taken continuously. However, the field depth of SEM is very short. Thus, at each step, it is required to stop the motor and refocus the lens on the specimen surface by a quick scanning. Following that, scan the crack tip again with higher resolution.

3.3. Image processing and Measurements

After SEM images are taken, some pre-processing are also needed to improve the image quality. Different from the optical image, SEM image consists of pixels calculated from the reflected electrons. As the electron reflection is not continuous in atomic length scale, the calculated pixels color changing is not smooth. The images taken under the visible light with wavelength much longer than atom scale length, the pixel colors are changing smoothly. The common process methods are noise reduction and smoothing. An example of comparison of images before and after processing is shown in Fig. 5, which is from the case study of steel.

Finally, crack tip opening displacement (CTOD) can be measured directly from the processed images. The definition of CTOD is defined as the distance of crack surface at the right angle edge from the crack tip, as Fig. 6(a) shows (Shih, 1981). Fig. 6(b) is an example SEM image with CTOD marked with white lines.

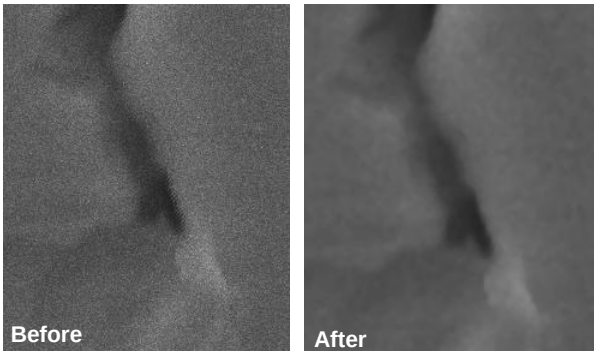

Fig. 5 Comparison of SEM image before and after processing

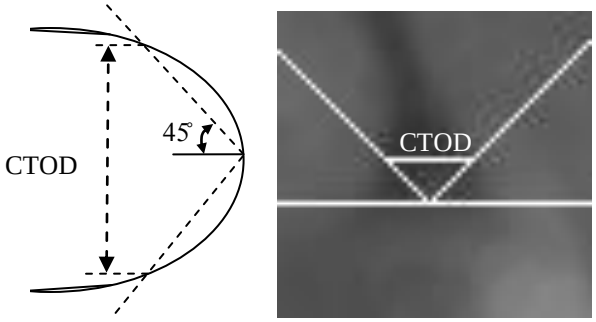

(a) CTOD definition (b) CTOD marked in SEM image

Fig. 6 CTOD measuring method and example

4. CASE STUDY

Using the above described in-situ optical and SEM testing methodology, two set of experiments are carried out on aluminum and steel, respectively. The objective is to investigate the plastic deformation and crack growth behavior and verify the classical mechanical models that have used widely for the plastic zone estimation and crack propagation law.

4.1. Case I: Aluminum 7075-T6

Aluminum 7075-T6 is a high strength to density material used for highly stressed structures but under strict weight requirement, such as automotive, marine, aircraft and many other daily staffs. In this case, three specimens are tested.

The chemical composition of this material is listed in Table 1. The aluminum is the balance in the total weight. The basic physical properties are listed in Table 2.

Element	Min	Max
Zn	5.1	6.1
Mg	2.1	2.9
Cu	1.2	2.0
Fe	0	0.5
Si	0	0.4
Mn	0	0.3
Cr	0.18	0.28

Table 1. Chemical composition Al 7075-T6 (weight, %)

Elastic Modulus /GPa	Yield Strength /MPa	Tensile Strength /MPa
71.7	502~516	573~582

Table 2. Basic mechanical properties of Al 7075-T6

Following the above discussed general methodology, the plastic zone size at each loading step can be estimated using the DIC analysis. The plastic zone size with the applied stress intensity factor is shown in Fig. 7. It could be easily found that during the unloading process, the reversed plastic zone size stops to grow at about 30% of the maximum loading. Crack closure is a sound reason for this behavior since the crack contact will reduce the stress intensity ahead of the original crack tip and plastic deformation disappears. Because as the crack closes, the crack surfaces are contacted to each other and it releases the reverse compression force from the crack tip region.

The theoretical value is calculated by Eq. (1) and (2), the value of geometry factor F is defined in Eq. (3) according to the ASTM standard E647-99.

$$F = 1.12 - 0.231\left(\frac{a}{W}\right) + 10.55\left(\frac{a}{W}\right)^2 - 21.72\left(\frac{a}{W}\right)^3 + 30.39\left(\frac{a}{W}\right)^4 \quad (3)$$

In order to full verify this hypothesis, the in-situ SEM experiment is taken to verify the crack closure and another crack parameter CTOD is measured directly.

Selected SEM images are shown in Fig. 8(a) and all the CTOD measurements are shown in Fig. 8(b). The crack closure is directly observed. The first two images shows that crack tip remain closed at two different loading levels. If further increase the loading level, crack becomes open. This explains why the plastic zone stops increases under in-situ optical testing. The testing results verify the crack closure hypothesis and indicate that the Eq. (1) is not applicable to aluminum alloys under the current investigation.

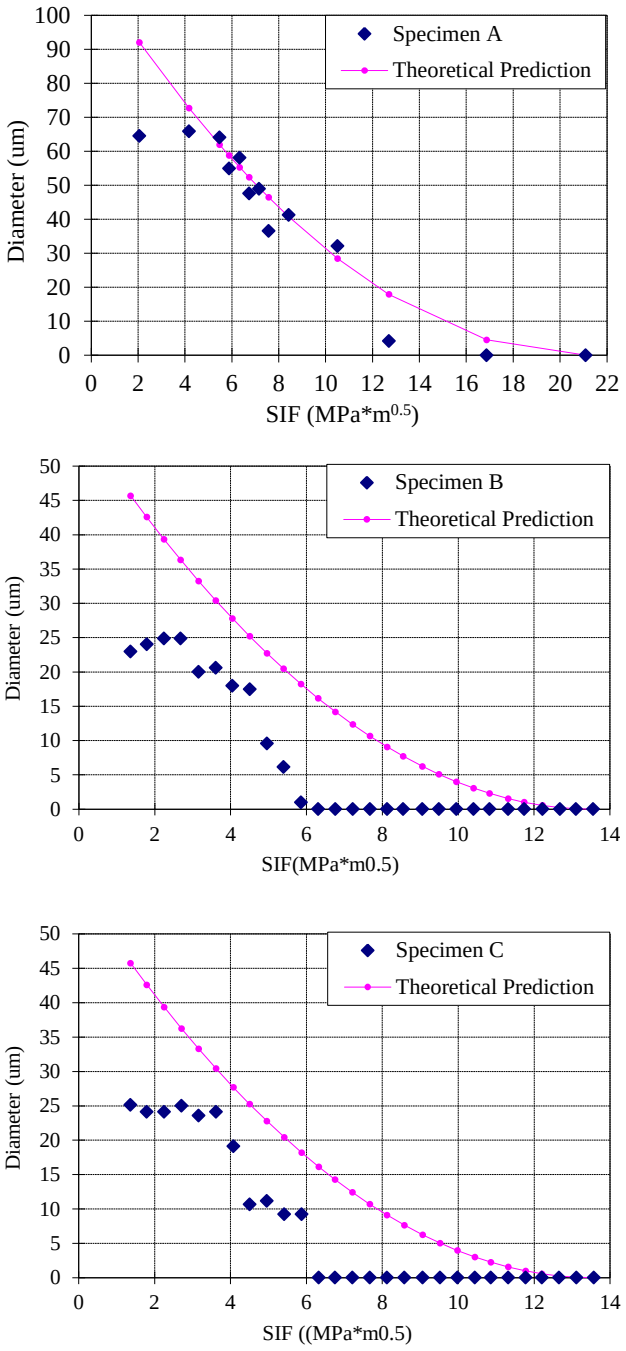

Fig 7 Plastic zone size of aluminum (Zhang & Liu, 2011)

4.2. Case II: Steel AISI 4340

AISI 4340 steel is a heat treatable, low alloy steel containing nickel, chromium and molybdenum. It is widely used in industry, such as aircraft landing gear, power transmission gears and shafts and other structural parts (after heat treatment and/or surface hardening treatment). The chemical

composition of this material and its basic physical properties are listed in Table 3 and 4.

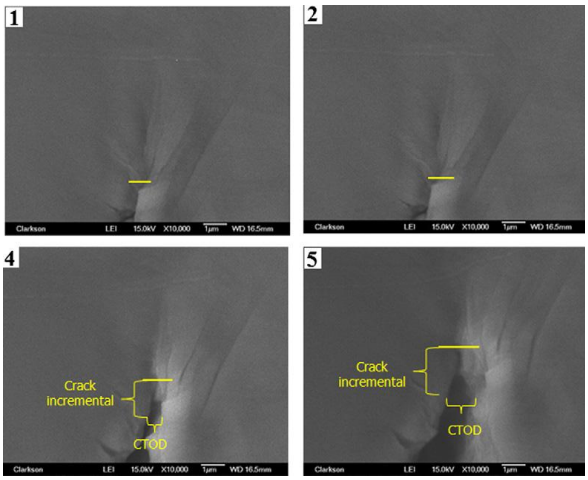

(a) Selected SEM images of aluminum during unloading process

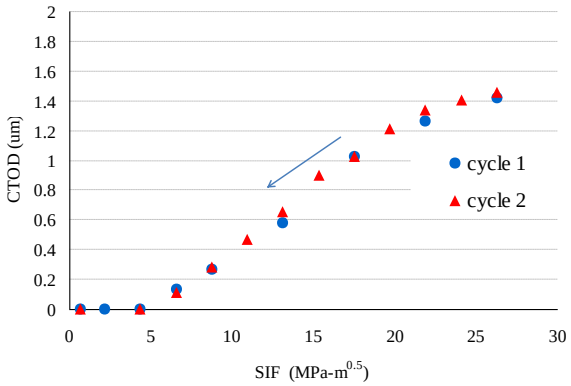

(b) CTOD during unloading process

Fig. 8 SEM images of aluminum in unloading process

The specimens are pre-cracked under load from 100 N to 1000 N at the frequency up to 5 to get an initial crack with length about 0.5 mm (excluding the notch length). A pre-cracked image is shown in Fig. 9.

After polishing, the average diameter of dark dots is about 15 μm, as shown in Fig. 10.

Then, the images are taken during the continuously loading or unloading process. In our test, the load profile starts from 100 N to 1000 N at step 50 N, as shown in Fig. 3. Finally, the plastic zone size variation during loading and unloading is obtained. In order to reduce the measurement noise, multiple tests have been performed. The result in Fig. 11 shows a good coherence of each test with the theoretic plastic zone size without consideration of plastic closure, i.e. the reversed plastic zone keeps increasing during the unloading process. This is very different compared to the results for aluminum alloys. The testing results indicate no crack closure during the entire unloading duration.

Element	Min	Max
C	0.38	0.43
Cr	0.7	0.9
Mn	0.6	0.8
Mo	0.2	0.3
Ni	1.65	2
P	0	0.035
Si	0.15	0.3
S	0	0.04

Table 3 Chemical composition of AISI 4340 steel

Elastic Modulus /GPa	Yield Strength /MPa	Tensile Strength /MPa
190~210	472.3	744.6

Table 4 Basic physical properties of AISI 4340 steel

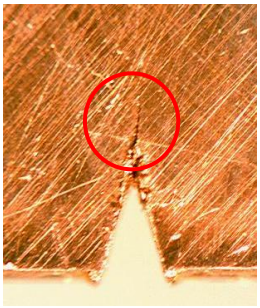

Fig. 9 Crack tip of steel specimen

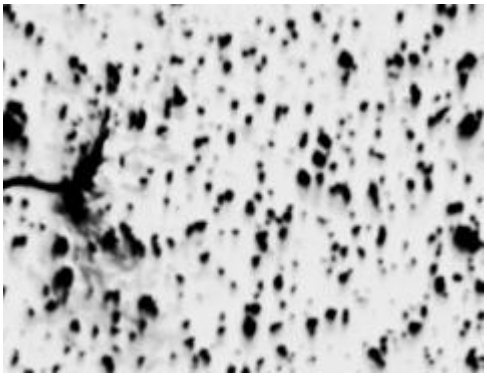

Fig. 10 Crack tip with markers for DIC process

In order to fully support this hypothesis, SEM images are taken one of the specimens and the CTOD in two unloading processes is obtained. The selected images are shown in Fig. 12(a) and the CTOD is shown in fig. 12(b). The images show that the crack edges do not contact to each other and the measured CTOD keeps growing during the whole unloading process according. The result proves that there is

no crack closure for ASNI 4340 steel under loading ratio 0.1 in the current investigation.

Compared with test on aluminum 7075-T6, ASNI 4340 steel does not have crack closure phenomenon under the loading profile with load ratio 0.1. Thus, it can be concluded that for different materials, crack closure does not always exist. This comparison also shows that the method proposed is a general method for crack fatigue mechanism investigation and model hypothesis verification.

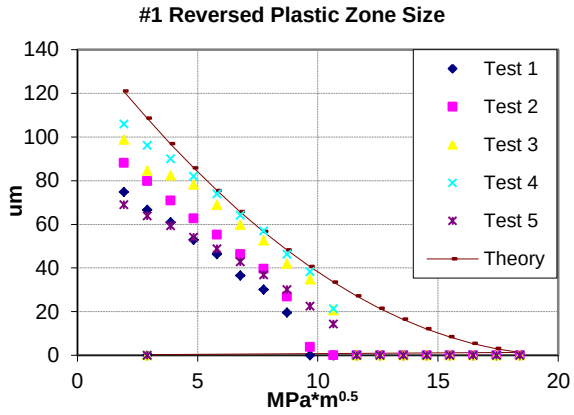

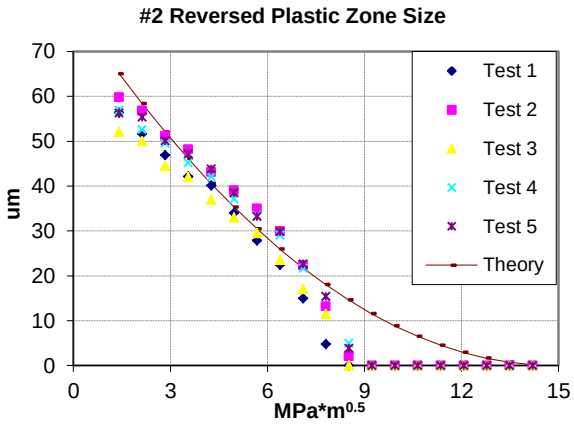

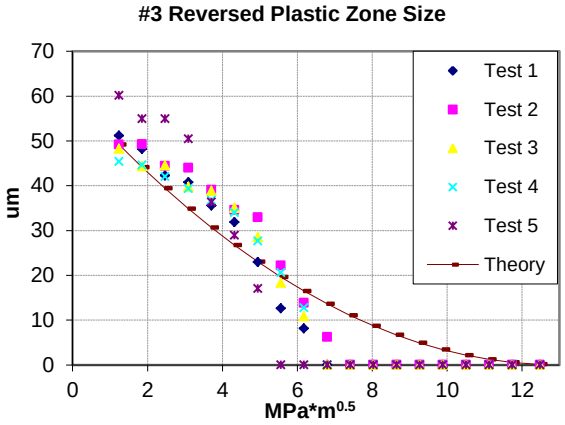

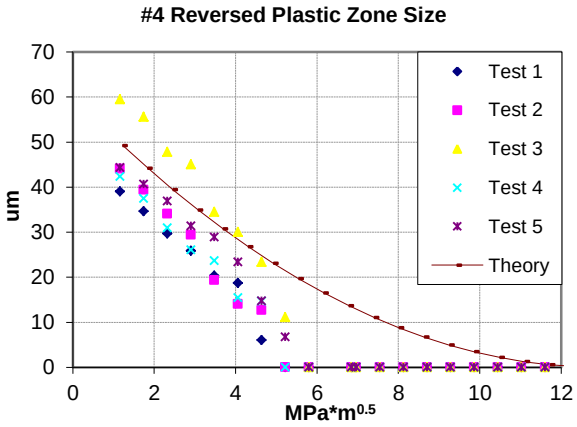

Fig. 11 Plastic zone size of steel specimens

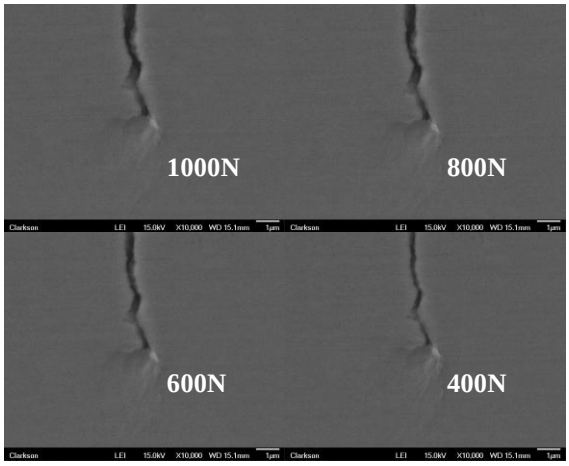

(a) Selected SEM images during the unloading process

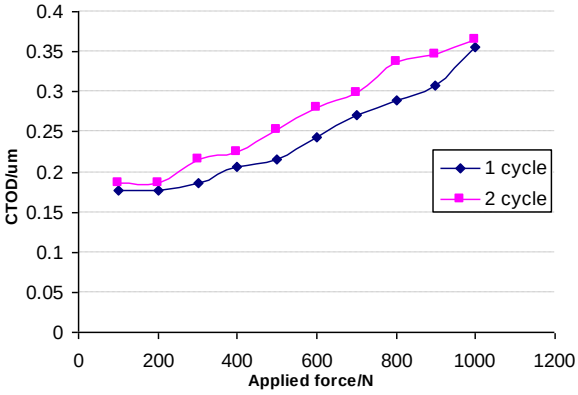

(b) CTOD during unloading process

Fig. 12 Crack tip condition of steel during unloading process

For aluminum 7075-T6, crack closure is observed and the opening stress is obtained. Thus it is suggested to use modified McClung's model (McClung & Sehitoglu, 1989)

to predict the crack growth rate provided by Wei (Zhang & Liu, 2011):

$$\rho_f = \begin{cases} 0 & K < K_{\text{open}} \\ \frac{1}{\pi}\left(\frac{K - K_{\text{open}}}{2\sigma_y + (\sigma_{\text{closure}} - \sigma_{\min})}\right)^2 & K \geq K_{\text{open}} \end{cases} \quad (4)$$

$$\rho_r = \begin{cases} \frac{1}{\pi}\left(\frac{K_{\max} - K_{closure}}{2\sigma_y}\right)^2 & 0 \leq K \leq K_{closure} \\ \frac{1}{\pi}\left(\frac{K_{\max} - K}{2\sigma_y}\right)^2 & K_{closure} < K \leq K_{\max} \end{cases} \quad (5)$$

where σ_{closure} is the crack closing stress and $\Delta K_{\text{eff}} = F \cdot \Delta\sigma_{\text{eff}}\sqrt{\pi a} = F \cdot (\sigma_{\max} - \sigma_{\text{closure}})\sqrt{\pi a}$. It can be noticed that Rice's model is a special case of McClung Model in that $\sigma_{\text{closure}} = \sigma_{\min}$.

The two materials show quite different behaviors under the same experiment condition. One probable reason is the difference of ductility. For 4340 steel, the failure elongation could be 12.2~22.0%, but for aluminum 7075-T6, that is only 5~8%, much more brittle than the former one. This could cause the fracture surface in aluminum more smooth than steel, thus the crack surface could not contact to each other during the unloading process. With the different behaviors for these two materials, different crack prognosis methods can be verified or new prognosis methods could be proposed, such as the one in Zhang and Liu's paper (Zhang & Liu 2011).

5. Conclusion and Future Work

This paper proposes a general methodology to verify the failure mechanism for physics-based mechanical damage prognosis. Testing under both optical microscope and SEM are discussed in detail. Imaging processing technique and advanced instrumentation provides a unique capability to investigate the mechanical damage behavior of structural materials.

Several conclusions can be drawn based on the current investigation:

- Multi-resolution in-situ testing and imaging analysis is powerful to explore the detailed mechanical deformation and damage accumulation behavior of investigated metals;
- Aluminum 7075 in the current investigation shows has crack closure under cyclic loadings and the reversed plastic zone stop growing after the crack closure
- Steel 4340 in the current investigation shows no crack closure and the plastic zone continues to grow during the entire unloading path
- Different mechanisms indicate that different prognosis models should be developed for these two materials, especially on the plastic zone calculation

The proposed methodology provides a general way to get the mechanical information of fatigue cracks. However, it does not only pertain to fatigue research, In the future, other metal failure mechanisms such as creep or brittle fracture mechanism will be studied using this method. In addition, composite materials failure mechanism such as delamination and matrix will also be studied using advanced 3D imaging technique, such X-ray computed tomography.

Acknowledgement

The research reported in this paper was supported by funds from Air Force Office of Scientific Research: Young Investigator Program (Contract No. FA9550-11-1-0025, Project Manager: Dr. David Stargel). The support is gratefully acknowledged.

References

Bouami, D., & De Vadder, D. (1986). Detection and measurement of crack closure and opening by an ultrasonic method. *Engineering Fracture Mechanics*, *23*(5), 913–920. DOI:10.1016/0013-7944(86)90101-3

Campbell, G., & Lahey, R. (1984). A survey of serious aircraft accidents involving fatigue fracture. *International Journal of Fatigue*, *6*(1), 25–30. DOI: 10.1016/0142-1123(84)90005-7

Farrar, C. R., & Lieven, N. a J. (2007). Damage prognosis: the future of structural health monitoring. *Philosophical transactions. Series A, Mathematical, physical, and engineering sciences*, *365*(1851), 623–32. DOI: 10.1098/rsta.2006.1927

Fleck, N., & Shin, C. (1985). Fatigue crack growth under compressive loading. *Engineering fracture mechanics*, *21*(1), 173–185. DOI: 0013-7944/85

Forsyth, P. J. E. (1962). A two stage process of fatigue crack growth. *Crack Propagation: Proceedings of Cranfield Symposium*. Cranfield (76–94), England: College of Aeronautics.

Laird, C. (1967). The influence of metallurgical structure on the mechanisms of fatigue crack propagation. *Fatigue Crack Propagation, ASTM STP*, *415*, 131–180.

Macha, D. E., Corbly, D. M., & Jones, J. W. (1979). On the variation of fatigue-crack-opening load with measurement location. *Experimental Mechanics*, *19*(6), 207–213. DOI: 10.1007/BF02324983

McClung, R. C., & Sehitoglu, H. (1989). On the finite element analysis of fatigue crack closure—1. Basic modeling issues. *Engineering Fracture Mechanics*, *33*(2), 237–252. DOI:10.1016/0013-7944(89)90027-1

Paris, P. C., Gomez, M. P., & Anderson, W. E. (1961). A Rational Analytic Theory of Fatigue. *Trend in Engineering*, *13*(1), 9–14.

Rice, J. (1968). A path independent integral and the approximate analysis of strain concentration by notches and cracks. *Journal of Applied Mechanics*, *35*, 379–386.

Riddell, W., Piascik, R., Sutton, M., Zhao, W., McNeill, S., & Helm, J. (1999). Determining Fatigue Crack Opening Loads from Near-Crack Tip Displacement Measurements. *ASTM SPECIAL TECHNICAL PUBLICATION*, *1343*, 157–174.

Sadananda, K. (1999). Analysis of overload effects and related phenomena. *International Journal of Fatigue*, *21*, 233–246. DOI:10.1016/S0142-1123(99)00094-8

Shih, C. F. (1981). Relationships between the J-integral and the crack opening displacement for stationary and extending cracks. *Journal of the Mechanics and Physics of Solids*, *29*(4), 305–326. DOI:10.1016/0022-5096(81)90003-X.

Shih, T. T., & Wei, R. P. (1974). A study of crack closure in fatigue. *Engineering Fracture Mechanics*, *6*(1), 19–32. DOI:10.1016/0013-7944(74)90044-7.

Singh, D. S., Srivastav, A., Gupta, S., Keller, E., & Ray, A. (2009). Ultrasonic measurement of crack opening load for life-extending control of mechanical structures. *2009 American Control Conference* (210–215), June 10-12. Piscataway, NJ, USA: IEEE. DOI: 10.1109/ACC.2009.5160021.

Wolf, E. (1970). Fatigue crack closure under cyclic tension. *Engineering Fracture Mechanics*, *2*(1), 37–45. DOI: 10.1016/0013-7944(70)90028-7.

Zhang, W., & Liu, Y. (2011). Plastic zone size estimation under cyclic loadings using in situ optical microscopy fatigue testing. *Fatigue & Fracture of Engineering Materials & Structures*, *34*(9), 717–727. DOI: 10.1111/j.1460-2695.2011.01567.x.

BIOGRAPHIES

Jian Yang is a Ph.D. candidate in the department of civil & environmental engineering at Clarkson University. He received his Bachelor's and Master's degrees in reliability & system engineering at Beihang University (Beijing University of Aeronautics and Astronautics), Beijing, China, 2008 and 2011 respectively. His research interests are fatigue propagation mechanics, simulation and test, structural health monitoring and prognosis.

Wei Zhang is a graduate research assistant in the department of civil and environmental engineering at Clarkson University. He received her B.S. degree in reliability engineering and M.S. degree in aerospace system engineering from Beihang University in China in 2005 and 2008, respectively. His research interests are fatigue analysis, structural dynamics, diagnosis and prognosis.

Yongming Liu is an associate Professor in the department of civil & environmental engineering. He completed his Bachelors` and Maters` degrees from Tongji University in China and obtained his Ph.D. at Vanderbilt University. His research interests include fatigue and fracture analysis of metals and composite materials, probabilistic methods, computational mechanics, and risk management. He is a member of ASCE and AIAA and serves on several technical committees on probabilistic methods and advanced materials.